View metadata, citation and similar papers at core.ac.uk
brought to you by CORE
provided by NASA Technical Reports Server

RECENT DEVELOPMENT OF Sb-BASED PHOTOTRANSISTORS IN THE 0.9- to 2.2-µM WAVELENGTH RANGE FOR APPLICATIONS TO LASER REMOTE SENSING

M. NURUL ABEDIN

Passive Sensor Systems Branch
NASA Langley Research Center
MS 468, 5 N. Dryden Street
Hampton, VA 23681

TAMER F. REFAAT

Science & Technology Corporation
NASA Langley Research Center
MS 468, 5 N. Dryden Street
Hampton, VA 23681

OLEG V. SULIMA

Department of Electrical Engineering
University of Delaware
Newark, DE 19716

UPENDRA N. SINGH

Systems Engineering Directorate
NASA Langley Research Center
MS 454, 5 N. Dryden Street
Hampton, VA 23681

We have investigated commercially available photodiodes and also recent developed Sb-based phototransistors in order to compare their performances for applications to laser remote sensing. A custom-designed phototransistor in the 0.9- to 2.2-µm wavelength range has been developed at AstroPower and characterized at NASA Langley's Detector Characterization Laboratory. The phototransistor's performance greatly exceeds the previously reported results at this wavelength range in the literature. The detector testing included spectral response, dark current and noise measurements. Spectral response measurements were carried out to determine the responsivity at 2-µm wavelength at different bias voltages with fixed temperature; and different temperatures with fixed bias voltage. Current versus voltage characteristics were also recorded at different temperatures. Results show high responsivity of 2650 A/W corresponding to an internal gain of three orders of magnitude, and high detectivity (D*) of 3.9×10^{11} cm.Hz^{½}/W that is equivalent to a noise-equivalent-power of 4.6×10^{-14} W/Hz^{½} (-4.0 V @ -20 ^{o}C) with a light collecting area diameter of 200-µm. It appears that this recently developed 2-µm phototransistor's performances such as responsivity, detectivity, and gain are improved significantly as compared to the previously published APD and SAM APD using similar materials. These detectors are considered as phototransistors based-on their structures and performance characteristics and may have great potential for high sensitivity differential absorption lidar (DIAL) measurements of carbon dioxide and water vapor at 2.05-µm and 1.9-µm, respectively.

Keywords: Photodiode, phototransistor, avalanche photodiode, Sb-based detector, responsivity, detectivity, dark current, noise-equivalent-power

I. Introduction

When selecting a detector, key parameters, such as spectral response, quantum efficiency, noise-equivalent-power (NEP), and gain must be considered in order to satisfy the requirements of the laser remote sensing systems. In general, p-i-n photodiodes and APDs are the detectors of choice for these systems. Antimonide (Sb)-based heterojunction phototransistor (HPT), as an alternative to p-i-n photodiode or avalanche photodiode (APD), stimulates a strong interest for 2 µm laser remote sensing applications[1-4]. Besides p-i-n

photodiodes and APDs, HPTs are also attracted a great attention to satisfy many of the detector requirements for applications to the laser remote sensing systems without excess noise and high bias voltages. HPT has an internal gain mechanism that allows increasing the output signal, to increase signal-to-noise ratio (SNR) based on optimum operating conditions. However, internal gain increases the noise, which increases NEP of the device for low signals and introduces high noise for high signals as well as slowing down the device. Even with this internal noise related gain, the HPT has a strong advantage over conventional APD and p-i-n diodes to operate at low bias voltage. But reduction of gain related noise is desirable, and research on different HPT structures indicates some important design considerations that can minimize device noise and increase SNR.

Earlier reports on phototransistors are made of Si[5], Ge[6], InGaAs/InP[7], and InGaAsP/InP[8] indicated that none of these materials is suitable for detection in the 0.6- to 2.4-μm range. Si has an upper limit wavelength at approximately 1.1-μm. Absorption in Ge also terminates before 2 μm, with an upper wavelength of approximately 1.9-μm. InGaAs/InP HPT operates in the 0.9- to 1.6-μm and quaternary InGaAsP on InP HPTs operates in the 0.9- to 1.3-μm wavelength range.

On the other hand, APDs are an integrated solid-state semiconductor device and the most common APDs, based on III-V compounds are fabricated using InGaAs on InP, and are operational in the range of 900 - 1600 nm[9-11]. InGaAsSb is a promising semiconductor for developing high gains 2 μm detectors. Several articles discussed the properties of this material and its application in p-n photodiode and APD fabrication[12-26]. The APD design most widely employed uses separate absorption and multiplication (SAM) layers. Andreev et al[16] and Mikhailova et al[17] demonstrated multiplication gain of ~45 (at -20.0 V and 23 ^{o}C) in 2-μm SAM APD and discussed the potential for higher gain of 200 - 500 at 78 ^{o}C with higher reverse bias voltage. Later, Shellenbarger et al[24] demonstrated high responsivity of ~7.2 A/W (at -11.0 V) and Johnson noise limited detectivity of $5x10^{10}$ cm.Hz^{½}/W in a 2 μm SAM APD. Sulima et al[26] measured responsivity as high as 43 A/W at 2.1-μm (at -6.7 V and room temperature) in SAM APD structure and also achieved relatively high responsivity 8.9 A/W at 2 μm (at -7.5 V and room temperature) in simple APD structure. Recently, Beck et al[27] has demonstrated responsivity of ~ 15 A/W in HgCdTe electron (e-) APD at 2 μm wavelength (biased at -7 V and 20 ^{o}C). HgCdTe e- APDs have demonstrated high responsivity in the 3- to 5-μm, but it produces low responsivity at the 2-μm region[27]. Even though HgCdTe detectors are efficient in the infrared range, due to the technology limitations of the HgCdTe system, researchers have looked to other III-V systems that provide much higher yield in terms of yield and operability. It is necessary to explore alternative material systems, which can absorb radiation in the 0.6 - 2.4 μm range and are compatible with the general requirements of a low-noise phototransistor. GaInAsSb/AlGaAsSb presents a strong candidate and published results show HPTs with quantum efficiencies of up to 60% (non-optimized, without AR coating)[3, 28-30] using liquid phase epitaxy (LPE) growth technique.

Recently, quaternary AlGaAsSb/InGaAsSb heterojunction phototransistors in the 1.0 to 2.2 μm wavelength range have been developed and fabricated at Astro-Power in collaboration with NASA Langley Research Center[3, 28-30]. These devices have been characterized at NASA Langley Research Center, and encouraging results including high responsivity, high detectivity, and relatively high dark current have been obtained. In this article, we report the characterization of commercial and custom-designed photodiodes and Sb-based phototransistors. Results include comparison of responsivity and dark current of a phototransistor with commercial photodiodes and detectivity (D*) of a phototransistor (HPT1:A1-a2) with InGaAs p-i-n photodiodes (G5852 and G5853) and HgCdTe p-n photodiode. Responsivity calibrations are carried out for a HPT1 and a p-i-n photodiode (D15-K204-13#8) at different bias voltages. This p-i-n photodiode consists of p+-InGaAsSb, π-InGaAsSb, and n-InGaAsSb layers on n-GaSb substrate. Experimental results of the HPT1 are compared with the results of the photodiode. In addition, responsivity variation at different temperatures and bias voltages were realized for two different phototransistors (HPT2:#A1-b1 and HPT3:#A1-d2). Spectral response and dark current measurements are performed of a HPT3 over a wide range of temperatures (70 ^{o}C to – 193 ^{o}C). The spectral response measurements are performed in the 0.6- to 2.4-μm wavelength range and the maximum responsivity 10^{4} A/W at 1.85-μm is

determined. Increasing responsivity of three orders of magnitude and increasing detectivity of several times have been determined and reported in earlier papers[3,28-29]. This was the first reporting of such high responsivity of 2650 A/W, high detectivity (D*) 3.9x10^{11} cm.Hz^{½}/W, and unprecedented gain of 2737 at 2 μm wavelength at -20 °C and -4.4 V. Lastly, we have tabulated the commercial and custom-designed two micron detectors and their manufacturers' information in Table I and also their performance characteristics comparison in Table II.

Finally, Sb-based phototransistors in the 0.6- to 2.4-μm development would enhance the capability of laser remote sensing, such as CO_2 profile measurements, wind measurements, aerosol and cloud measurements at 2-μm. These measurements are needed to better understand the global atmosphere. The 0.6- to 2.4-μm region contains trace gases such as H_2O, CO, CH_4, NO, and SO_2 that can be used in active and passive remote sensing to understand many atmospheric processes linked to climate change. However, there are no suitable detectors with high responsivity (QE) and low noise in the 0.6- to 2.4-μm range in general, and in the 2-μm range in particular, to take advantage of laser developments in the 2-μm region. Development of Sb-based phototransistors will enhance the capability for passive remote space sensing imaging systems and enable major advances in Astronomical, Earth, and planetary remote sensing instruments. This new detector will enhance the capability for active remote sensing of CO_2 and water vapor at 2.05 and 1.9 μm, respectively.

Table I Commercial and custom-designed detectors sensitive at the wavelength of 2 μm used for comparison with the new phototransistor

Manufacturer	Existing Devices	Custom-Designed Devices
Hamamatsu Corp	InGaAs (2.3 μm cutoff)	
Hamamatsu Corp	InGaAs (2.6 μm cutoff)	
Judson Technologies	HgCdTe (2.7 μm cutoff)	
Astro-Power, Inc	InGaAsSb (2.1 μm cutoff)	
Astro-Power, Inc		InGaAsSb (2.1 μm cutoff)
Rensselaer Polytechnic Institute		InGaAs/GaSb (2.25 μm cutoff)
Rensselaer Polytechnic Institute		InGaSb/InGaSb (2.08 μm cutoff)

II. Sb-based detector fabrication methods and procedures

The phototransistor used in this study consists of AlGaAsSb and InGaAsSb layers with band gaps of around 1eV and 0.55 eV as shown in Figure 1. These layers were grown on lattice-matched GaSb substrate by using liquid-phase epitaxy through a horizontal slide boat technique[28]. The graphite slide boat was situated in a sealed quartz tube mounted in a three-zone tube furnace, which was controlled by programmable microprocessor. The epitaxial layer was grown by passing palladium-diffused hydrogen at atmospheric pressure with a flow rate of 300 ml/min. The n-type GaSb (100) substrates with an area of 14x14 mm^2 were doped to 3-5 x 10^{17} cm^{-3} with tellurium.

The epitaxial InGaAsSb layers were grown using solutions of indium (x_{In}=0.59), gallium (x_{Ga}=0.21) and antimony (x_{Sb}=0.20), where x_i is the atomic fraction of the element i (In, Ga, and Sb) in the solution. High purity (99.9999%) indium, gallium, and antimony elements were employed without any intentional doping of the melts. Prior to growth, the melts are baked at 700°C for 15 hours in hydrogen to de-oxidize the melt components and to outgas residual impurities. After the baking and cooling, an un-doped

polycrystalline InAs "float" wafer is placed on top of the melt and then, the boat is heated to 530°C. During this process, arsenic from the float InAs wafer is added to the melt through the partial dissolution of the wafer. The melt is equilibrated for 1 hour at 530°C and then cooled down to the growth temperature. At 515°C, the substrate is brought in contact with the melt to grow an $In_{0.15}Ga_{0.85}As_{0.17}Sb_{0.83}$ collector layer with an electron concentration of 1- 4 x 10^{16} cm^{-3}. In general, unintentionally doped $In_{0.15}Ga_{0.85}As_{0.17}Sb_{0.83}$ layers can be either of n- or p-type. . Addition of a small amount of rare earth elements, such as Gd or Yb to the In-Ga-As-Sb melt results in a low doped n-type $In_{0.15}Ga_{0.85}As_{0.17}Sb_{0.83}$ layer. Thus, by regulating the concentration of Gd or Yb, one can grow both n-type (collector) and p-type (the narrow bandgap part of the base) InGaAsSb layers with a low (down to 1-4 x 10^{16} cm^{-3}) concentration of majority carriers.

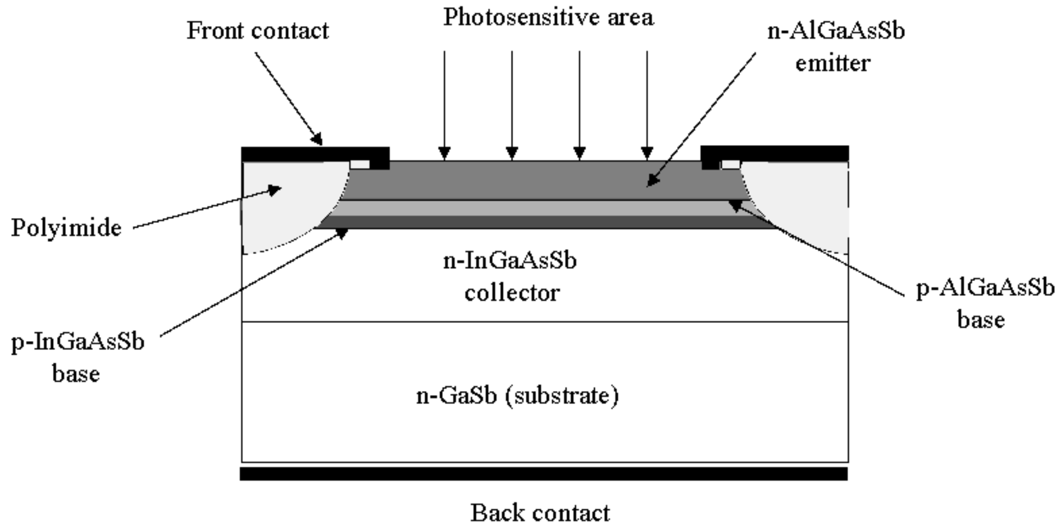

Fig. 1 Schematic of AlGaAsSb/GaInAsSb phototransistor layered structures[30].

Epitaxial AlGaAsSb layers (the wide bandgap part of the base, and emitter) were grown from the melt, which consists of gallium (x_{Ga}=0.959), antimony (x_{Sb}=0.013), and aluminum (x_{Al}=0.028). Similarly to the growth of the InGaAsSb layers, arsenic is added to the solution from an un-doped polycrystalline float wafer (in this case GaAs), which is partially dissolved at the growth temperature. The $Al_{0.28}Ga_{0.72}As_{0.014}Sb_{0.986}$ layers were grown on the InGaAsSb layers at 509°C. The p-type AlGaAsSb layer was grown from the melt without any intentional doping. To obtain the n-type AlGaAsSb emitter layer, Te-doped GaSb with a doping concentration of 2 x 10^{18} cm^{-3} was added to the melt. The thickness of the epitaxial layers is regulated by the time of the melt-substrate contact. After the end of the growth the melts are wiped from the substrate.

As described above, the fabricated phototransistors are composed of an n-type AlGaAsSb emitter, p-type base comprising of AlGaAsSb and InGaAsSb layers, and an n-type InGaAsSb collector. A 400-μm in diameter mesa-phototransistors with a 200-μm diameter of active area were fabricated using photolithography and wet chemical etching. Au/Sn or Ti/Ni/Au metal contacts (ohmic) were deposited at the backside (planar) and front side (annular) of the phototransistors. A polyimide resin was applied on the front surface of the device to provide mesa isolation, planarization of the front surface, and mesa wall passivation. After dicing, single devices with an area of 1-mm^2 were mounted to TO-18 header, contacted using silver epoxy, and wire-bonded. No antireflection coatings were applied.

III. Detector Characterization Setup

Figure 2 shows characterization setup[31] to obtain the detector characteristics in order to compare its performance with the requirement of the specific-application. The characterization experiments included

spectral response, dark current and noise measurements, and its variation with bias voltage and temperature. The setup is divided into three sections: I. an optical section, II. detector control section and III. electrical section. The optical section is used to apply a uniform, monochromatic radiation onto the detector, with known intensity. Section II is utilized to control the temperature and also apply bias to the detector. The electrical section mainly measures the detector output, corresponding to a certain operating conditions.

The radiation source consists of a current controlled quartz halogen lamp, the output of which is modulated using an optical chopper. The chopping frequency is set to a prime number of 167 Hz to reduce the effect of pickup noise. A monochromator is used to separate the radiation into its spectral components with a 40 nm maximum resolution as set by the input/output slits and the grating (1.25 mm input and output slits and 1200 Grove/Line grating). Higher order dispersion of the shorter wavelength is blocked using appropriate high-pass filters, while a diffuser is mounted at about 10 cm from the detector to insure radiation uniformity. An optical microscope was used to set the location of the optical axis and to fix the distance between the radiation source and the sensitive area of the detector. The radiation uniformity is estimated to be less than 1% along a 15 mm^2 area at the detector location.

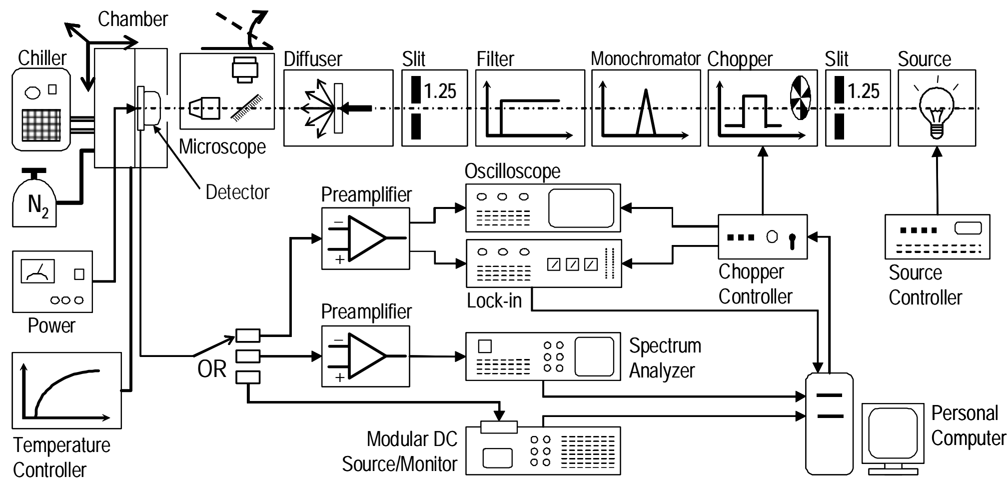

Fig. 2. Characterization Setup for detector dark current, spectral response and noise measurements at different temperatures and bias voltages[31].

The detector output current is converted into voltage signal using the pre-amplifier (Stanford Research Systems; SR570), the output of which is applied to a lock-in amplifier (Optronic Laboratories, Inc.; OL 750-C), oscilloscope (Agilent; infiniium) or spectrum analyzer (Stanford Research Systems; SR785), for spectral response and noise measurements. For dark current measurements, a modular dc source/monitor (Hewlett Packard; 4142B) is connected directly to the detector. The chopper controller synchronizes the applied optical signal, if any, with the data acquisition device through the personal computer. To bias the detector, the pre-amplifier is used for voltages in the 0 to 4 V range while the external dc power supply is used for higher voltages. The detector is mounted inside a chamber that controls its temperature and provides mechanical support. The temperature is controlled using thermoelectric coolers and a thermistor, located as close as possible to the device. Detector temperature can be set between 70 ^{o}C and –193 ^{o}C with 0.1 ^{o}C resolution. Water circulation through a chiller removes excess heat accumulation and nitrogen purging prevents water condensation and ice formation on the detector surface at lower temperatures. The mechanical mount allows detector alignment within 10 μm resolution.

IV. Characterization Results and Discussions

Several detectors at 2-μm wavelength range have been characterized to measure the responsivity, dark current, and noise. A PbS standard detector is employed to obtain the spectral responsivity of the test detector. The output signal of the test detector as a function of wavelength is acquired and then, compared with that of a spectrally calibrated PbS detector. The spectral responsivity, $R_T(\lambda)$ (in A/W), of the test detector is determined by using the following equation[30]:

$$R_T(\lambda) = \frac{V_T(\lambda)}{V_{PBS}(\lambda)} \cdot \frac{A_r}{G} \cdot R_{PBS}(\lambda) \qquad (1)$$

where V_{PbS} is the PbS photodiode response (in V), V_T is the test detector response (in V), A_r is the ratio of the PbS detector area to the test detector area, G (in V/A) is the preamplifier gain setting, and $R_{PbS}(\lambda)$ (in V/W) is the spectral responsivity of the PbS detector.

Figure 3 shows the spectral response of the commercially available and custom-designed detectors in the 1- to 2.8-μm region, with 40 nm spectral resolution, obtained at zero bias voltage and 20 ^{o}C[32]. The highest responsivity at 2 μm was achieved by the InGaAs (2.6-μm) p-i-n detector (G5853), while the InGaAs (2.3-μm), InGaAs (2.6-μm), InGaSb, InGaSb/GaSb, InGaAsSb and HgCdTe had their peaks at about 2.1, 2.4, 1.9, 2.12, 2.0, and 2.5-μm. The InGaAsSb detector indicated responsivity enhancement in the 1.8- to 2.2-μm spectral range, i.e. 400 nm narrow spectral period. The reduction in the responsivity at wavelengths shorter than 1.8-μm has the advantage of reducing the background signal which increases the detector dynamic range for the DIAL return signal. Besides, this might lower the restriction regarding the narrow band pass filter required with the DIAL detection. The spectral response of the InGaSb/GaSb detector shows two distinctive peaks at 1.7 and 2 μm wavelengths, corresponding to the GaSb and InGaSb bandgap energies. Although replacing the substrate of the InGaSb detector indicated lower responsivity, it enhances the dark current and the noise contents of the device[3].

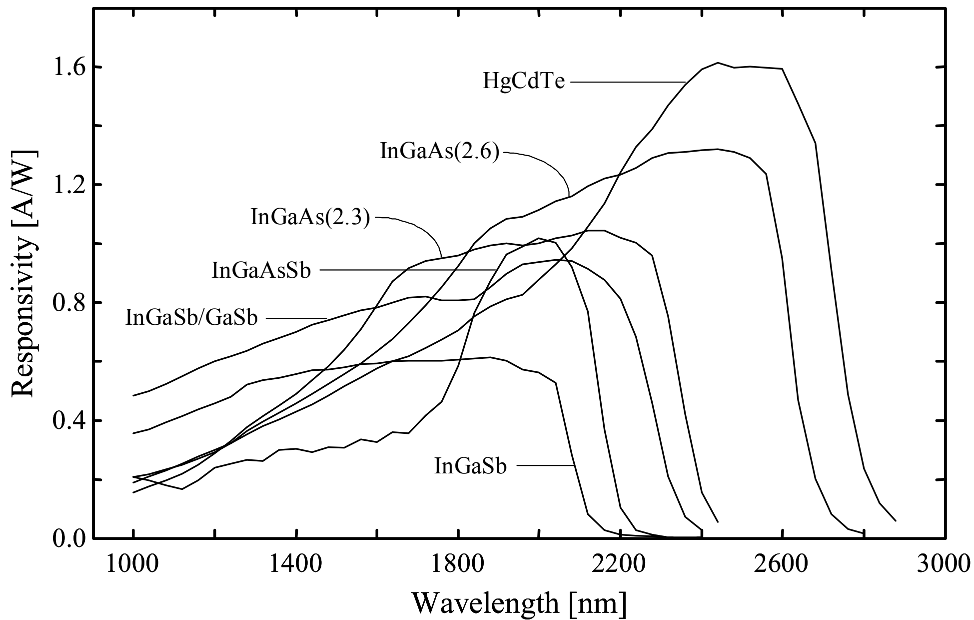

Fig. 3. Comparison of spectral response measurements for commercial and custom-designed detectors[32].

Figure 4 shows the dark current variation with bias voltage for the different detectors, obtained by measuring the current-voltage characteristics of the device in a dark condition at a temperature of 20ºC[32]. The InGaAs (2.3-µm) detector (G5852) indicated the lowest dark current even at higher bias voltages. The highest current obtained from InGaSb/GaSb detector is mainly due to the lattice mismatch which was improved by two orders of magnitude by using the lattice matched InGaSb substrate. InGaAsSb p-n diode showed higher dark current similar as InGaSb/InGaSb p-n diode, but InGaAs (2.6-µm) showed higher dark current as compared to InGaAs (2.3-µm). At low bias voltages, the dark current of the phototransistor is close to that of the InGaAs (2.6-µm) diode, as well as of the HgCdTe diode and, however, at higher bias voltages it exceeds the dark current if the InGaAs (2.6- µm) device.

The dark current (I_d) and the noise current I_n of the phototransistor are dependent on applied voltage and temperature. The noise spectrum was obtained at different bias voltages (0.1 V step) in the 0 to 100 KHz frequency band used for the commercial detectors and the phototransistors. The total noise voltage spectral density was calculated by integrating the spectrum and normalizing to the bandwidth. The voltage spectral density was converted to a current spectral density using the preamplifier gain setting. These data were corrected for background and preamplifier noise. As might be expected, the phototransistor exhibited an increase of I_d (Fig.4) and I_n with voltage and temperature. Thus, both temperature dependencies of R and I_n (I_d) should be considered for optimum operation of the phototransistor. For the measured devices the temperature dependence of I_n (I_d) was stronger than that of R, and the value of detectivity D^*, which is dependent on both R and I_n and is determined[28] as

$$D^*(T,V) = R(T,V) \cdot \sqrt{A} / I_n(T,V), \tag{2}$$

where A is the detector area, was higher at –20ºC. Comparison with the best of the tested commercial detectors shows that the phototransistor reported here achieves more than a 4 times higher D* at 4 V and –20ºC in Fig.5.

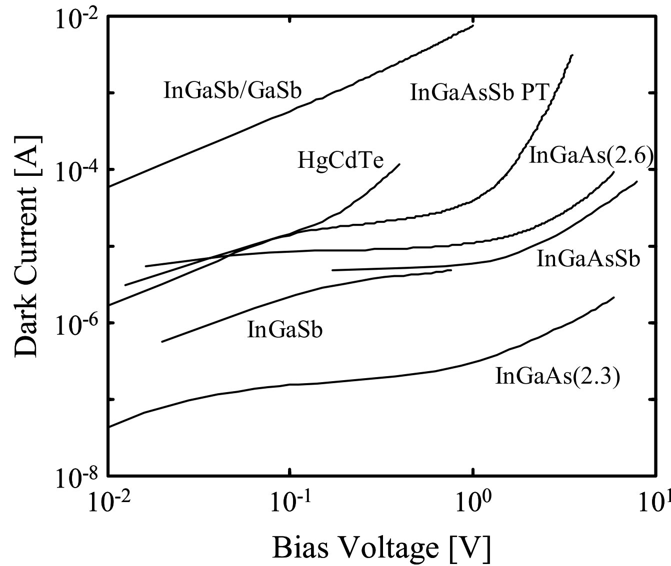

Fig. 4. Dark current measurements of commercial and custom-designed detectors[32].

Fig. 5 shows the detectivity calculation of a phototransistor (sample A1-a2) as compared to the state-of-the-art, 1 mm diameter InGaAs (2.3-µm), InGaAs (2.6-µm), and HgCdTe photodiodes, listed in table II. Detectivity calculation was obtained using noise measurements in the dark conditions and spectral response

data (detail discussion in ref. 28). The figure also compares the results with the temperatures between 20°C and -20°C and results obtained at -20°C, was only considered for A1-a2 sample to emphasis cooling improvements. Cooling down the device reduces the dark current allows for higher voltage operation, and results in increased responsivity. Therefore, higher detectivities are observed at lower temperatures. For the shown curve (-20°C), the peak detectivity as high as 4.0×10^{11} cm.Hz^{½}/W is determined at 4.0 V bias. An optimization would be required to identify a suitable operating temperature while avoiding the responsivity drop due to the cut-off wavelength shift at lower temperatures. The operating bias voltage for the commercial detectors was 1 V as specified by the manufactures. It should be noted that increasing the bias voltage for the commercial detectors significantly increases the noise, leading to detectivity deterioration as shown in Fig. 5[28].

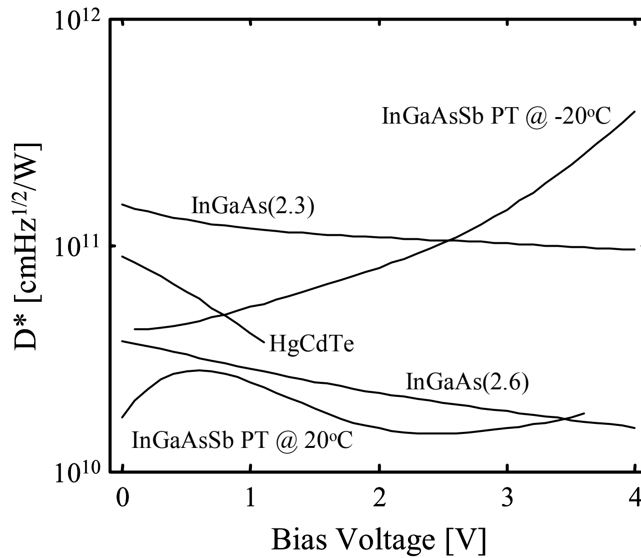

Fig. 5. Comparison of detectivity for commercial detectors and custom-designed phototransistor (HPT1: A1-a2)[28].

Figure 6 shows the spectral responsivity of the InGaAsSb p-i-n photodetector and of the AlGaAsSb/InGaAsSb phototransistor as a function of applied bias at 20°C. As expected, the responsivity of

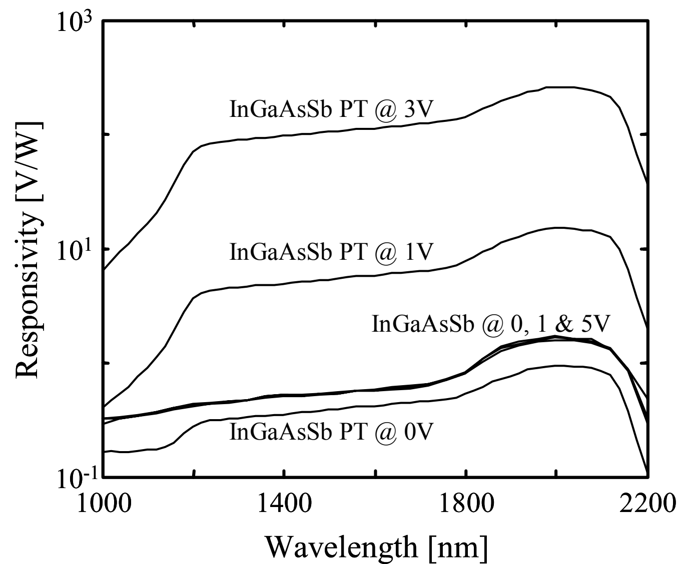

Fig. 6. Comparison of spectral response for InGaAsSb between a photodiode and a phototransistor (HPT2: A1-b1).

the phototransistor has a strong bias dependence. Responsivity grows by more than two orders of magnitude with the bias voltage, V (V_{ce}: collector-emitter voltage), from 0 to 3.0 V. For a p-i-n photodiode, a small increase of the responsivity with applied voltage can be explained by the expanding space charge region. Finally, the responsivity for the HPT is much improved at reverse bias as compared to the p-i-n photodiode. The measured responsivity for the HPT at 3.0 V is 250 A/W and this value is about 210 times higher than that of the p-i-n photodiode.

Figure 7 shows the responsivity variation with the collector-emitter voltage at different temperatures for a phototransistor sample HPT2. As a general trend, sharp increase in the responsivity at lower bias voltage is observed, followed by gradually increment at higher voltage. Responsivity as high as 2650 A/W, corresponding to an internal gain of 2737, was measured with phototransistor HPT2 at 2.05 µm, -20°C and 4.4 V. The quantum efficiency has been calculated for 0.0 V bias at 20°C and the quantum efficiency plot is shown in the same Figure. The peak quantum efficiency 58% is obtained at 2 µm and 50% of peak quantum efficiency is determined at 2.15-µm.

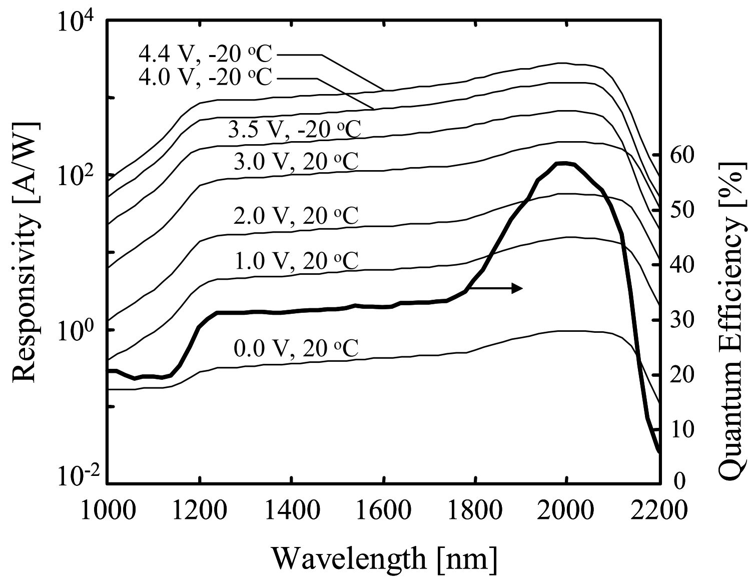

Fig.7. Comparison of spectral response at different temperatures and bias voltages (HPT2: A1-b1). Determined quantum efficiency at 0.0 V and 20°C[3].

One aspect of detectors that need to be addressed is the extreme temperature conditions. Therefore, we have carried out comprehensive device characterization, including responsivity and dark current at NASA LaRC at 70°C to -193°C. Figure 8 shows the responsivity variation in the 0.6- to 2.4-µm wavelength range with the temperature at different collector-emitter voltages for a phototransistor sample HPT3. The results indicate complicated temperature dependence with a low responsivity peak around -193°C at 0.0 V and increases more at higher temperatures and higher bias voltages. Increasing the bias voltage regains the 2 µm sensitivity and very high responsivity around 10000 A/W is observed at -193°C with 5.0 V bias voltage at 1.9-µm. This is the highest responsivity for this Sb-based phototransistor ever reported at this wavelength range.

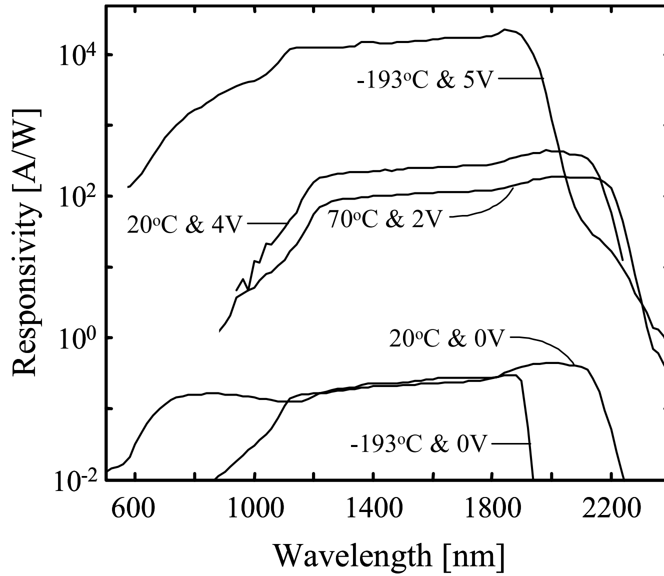

Fig. 8 Spectral response variation at different bias voltages and temperatures (HPT3: A1-d2)

Fig. 9 shows the emitter dark current variation with the collector-emitter voltage at different temperatures of HPT3. Emitter dark current was obtained by I-V measurements in dark conditions by applying the bias voltage to the emitter while the collector contact connected to the ground. Two current regions were observed in these characteristics. The first region, where 0- to 1.5-V was applied, is characterized by a relatively low current with strong temperature dependence. At higher voltage, above 1.5 V, a sharp increase in the dark current with lower temperature dependence and high current-voltage linearity is observed. Emitter dark current measurements reveal the absence of any avalanche gain[3]. Finally, a comparison of commercial and custom-designed detectors' parameters and figure-of-merits is tabulated in Tabe II.

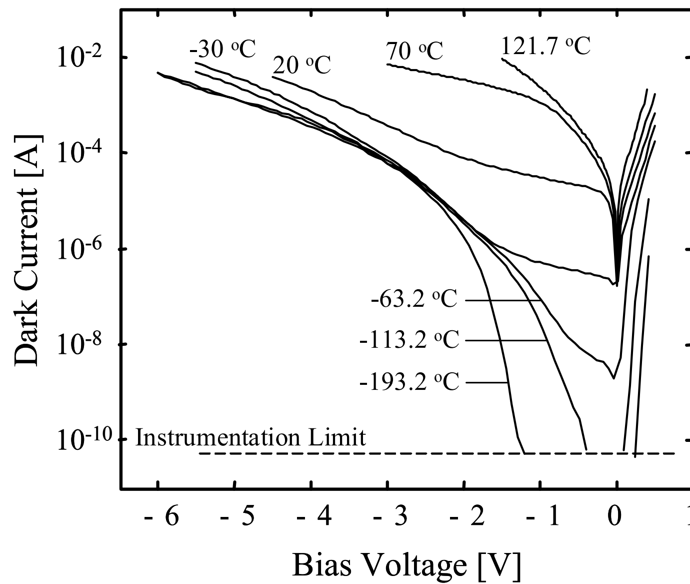

Fig. 9. Dark current measurements of custom-designed phototransistor at different temperatures (HPT3: A1-d2)

V. Anticipated advantages compared to existing technologies

The relevance of this work to advance measurement used in lidar remote sensing applications must have high gain and low noise. Several types of detectors might be suitable in the spectral range from visible- to 1.8-µm. However, detectors based on InGaAsSb and InGaAs materials were evaluated to obtain lower gain as compared to Si APD; and InGaAsSb detector has higher noise as compared to InGaAs detector and results were reported[31,33-34]. On the other hand, the band gap of the active layers in AlGaAsSb/InGaAsSb phototransistors may be tuned in a way to provide maximum detectivity at a certain wavelength in a wide range of wavelengths between 0.6- to 2.4-micron.. We have identified a high performance phototransistor with the optimum spectral response for the DIAL application. This technology component development will increase instrument signal-to-noise ratio (SNR) and enhance sensitivity.

The detector component development is relevant to the Science missions and the exploration systems. This technology component is based on III-V material system, which is much more technologically advanced, compared to the II-VI material system. Hence, it is easier to fabricate III-V-based devices with high operability, good uniformity, high yield, and also lower cost. All these advantages will decrease the cost of the DIAL system. This technology component has the potential to influence many remote sensing applications. Single element phototransistor for the DIAL instrument will operate in the spectral range 0.6- to 2.4-µm and extend this technology to 2-D array for next generation 3-D Lidar remote sensing application.

Table II Comparison of commercial and custom-designed detectors' performances at the wavelength of 2 µm and at -20 °C

Detector	Diameter	Responsivity	Quantum Efficiency	Noise Current Density (I_n)	Noise Equivalent Power (NEP)	Detectivity (D*)
Unit	µm	A/W	%	A/√Hz	W/√Hz	cm.√Hz/W
InGaAs (Off the Shelf)	1000	1.0004	62.1	$7.3x10^{-13}$	$7.3x10^{-13}$	$1.2145x10^{11}$
InGaAs (Off the Shelf)	1000	1.1134	70.4	$3.5x10^{-12}$	$3.1x10^{-12}$	$2.8192x10^{10}$
HgCdTe (Off the Shelf)	1000	0.8761	54.4	$1.9x10^{-12}$	$2.2x10^{-12}$	$4.0862x10^{10}$
InGaAsSb (Off the Shelf)	200	1.018	63.2	$6.2x10^{-12}$	$6.1x10^{-12}$	$2.9104x10^{9}$
InGaSb/GaSb (Custom-designed)	800	0.9374	58.2	$7.8x10^{-12}$	$8.3x10^{-12}$	$8.5201x10^{9}$
InGaSb (Custom-designed)	200	0.5637	35.0	$4.3x10^{-13}$	$7.6x10^{-13}$	$2.3418x10^{10}$
InGaAsSb (Custom-designed)	200	2646	58	$12.2x10^{-11}$	$4.6x10^{-14}$	$3.9x10^{11}$

VI. Conclusions

The custom-designed phototransistor has been developed at AstroPower under NASA contract. The phototransistor has been characterized at NASA LaRC to measure the responsivity, dark current, and noise. Device performances have been demonstrated in the laboratory to determine responsivity, detectivity, and noise-equivalent-power. InGaAs and HgCdTe detectors were considered in this study as samples of the

current well developed commercially available technology. Newly developed InGaAsSb and InGaSb detectors were obtained and characterized. The detector manufacturers' information are given in table I. Table II summarizes some additional detector performances at the 2 μm wavelength. From the table we can conclude that the quantum efficiency requirement can be simply met with current available technology. Future work is required to reduce the detectors noise and increase their gain. Results from a HPT show high responsivity 2650 A/W corresponding to an internal gain of 2737, high detectivity (D*) 3.9×10^{11} cm.Hz½/W that is equivalent to a noise-equivalent-power of 4.6×10^{-14} W/Hz½. This phototransistor was also characterized at extreme temperature condition and observed its performance consistency operating at this temperature range. The maximum responsivity of 10000 A/W at -193°C and 5.0 V bias and also relatively low dark current at -193°C are determined. This is the highest responsivity ever reported in the 0.6- to 2.4-μm wavelength range for the Sb-based material system. These detectors are considered as phototransistors based-on their performance characteristics and may have great potential for lidar remote sensing applications and this technology will improve the capabilities to measure atmospheric pollutants for future Earth Science measurements. This technology has also tremendous applications to NASA's Human and Robotic Exploration Program for use in 3-D imaging Focal Plane Arrays for planetary mapping and robotics navigation.

Acknowledgement

This work is supported by Laser Risk Reduction Program under NASA's Earth Science Technology Office and NASA's Enabling Concepts & Technologies Program. The authors acknowledge George Komar, Chris Moore, and Frank Peri for their constant support.

References

1. P. Ambrico, A. Amodeo, P. Girolamo, and N. Spinelli 'Sensitivity analysis of differential absorption lidar measurements in the mid-infrared region', Applied Optics, 2000, 39, (36), pp. 6847–6865.
2. S. Ismail, G. J. Koch, B. W. Barnes, N. Abedin, T. F. Refaat, J. Yu, S. A. Vay, S. A. Kooi, E. V. Browell, U. N. Singh, "Technology Developments for Tropospheric Profiling of CO2 and Ground-based Measurements", Proceedings of the 22nd International Laser Radar Conference, pp 65-68 (2004).
3. T.F. Refaat, M.N. Abedin, O.V. Sulima, S. Ismail, and U.N. Singh, "AlGaAsSb/InGaAsSb Phototransistors for 2-μm Remote Sensing Applications", Optical Engineering, Vol. 43(7), 1647-1650, 2004.
4. T.F. Refaat, M.N. Abedin, O.V. Sulima, U.N. Singh, and S. Ismail, "Novel Infrared Phototransistors for Atmospheric CO2 profiling at 2 μm Wavelength", International Electron Devices Meeting (IEDM), in San Francisco, CA, December 12 – 15, 2004.and IEDM Tech. Dig., pp. 355-358, December 2004.
5. M.A. Schuster and G. Strull, "A monolithic mosaic of photon sensors for solid-state imaging applications", IEEE Trans. Electron Devices ED-13, p. 907-912 (1966)
6. J.N. Shive, "The properties of germanium phototransistors", J. Opt. Soc. Am. 43, p. 239 – 244 (1953).
7. J.C. Campbell, A.G. Dentai, C.A. Burrus, and J.F. Ferguson, "InP/InGaAs heterojunction phototransistors", IEEE J. Quantum Electronics, 17, 264-269 (1981).
8. M. Tobe, Y. Amemiya, S. Sakai, and M. Umeno, "High-sensitivity InGaAsP/InP phototransistors", Appl. Phys. Lett., 37, 73-75 (1980).
9. V. Diadiuk, S.H. Groves, C.E. Hurwitz, and G.W. Iseler, "Dark-current, high gain GaInAs/InP avalanche photodetectors," IEEE J. Quant. Electronics, QE-17 (2), 260-264 (1981)

10. J.C. Campbell, A.G. Dentai, W.S. Holder and B.L. Kasper, "High-performance avalanche photodiode with separate absorption 'Grading' and multiplication regions", Electron. Lett. 19, 818-820, 1983.
11. K.K. Loi and M. Itzler, "Avalanche photodetectors for 10 Gb/s fiber optics receivers," Compound Semiconductor, 6(3), pp. 1-3, April 2000.
12. J. C. DeWinter, M. A. Pollack, A. K. Strivastava and J. L. N. Zyskind, "Liquid phase epitaxial GaInAsSb lattice matched to (100) GaSb over the 1.71 to 2.33 μm wavelength range", *Journal of Electronic Materials*, 14(6), 729-747, 1985.

13. M. Astles, H. Hill, A. J. Williams, P. J. Wright and M. L. Young, “Studies of the $Ga_{1-x}In_xAs_{1-y}Sb_y$ Quaternary alloy system I. Liquid-phase epitaxial growth and assessment”, *Journal of Electronic Materials*, **15**(1), 41, 1986.
14. I. A. Andreev, M. A. Afrailov, A. N. Baranov, M. A. Mirsagatov, M. P. Mikhailova and Yu. P. Yakovlev, “Avalanche multiplication in photodiode structures using GaInAsSb solid solutions”, *Soviet Technical Physics Letters,* **13**(4), 199-201, 1987.
15. J. Benoit, M. Boulou, G. Soulage, A. Joullie and H. Mani, “Performance evaluation of GaAlAsSb/GaInAsSb SAM-APDs for high bit rate transmission in the 2.5µm wavelength region”, *Journal of Optical Communication*, **9**(2), 55-58, 1988.
16. I.A. Andreev, M.A. Afrailov, A.N. Baranov, M.A. Mirsagafov, M.P. Mikhailova, and Y.P. Yakoviev, “GaInAsSb/GaAlAsSb avalanche photodiode with separate absorption and multiplication regions”, Sov. Tech. Phys. Lett. 14(6), pp. 435-437 (1988).
17. M.P. Mikhailova, I.A. Andreev, A.N. Baranov, S.V. Mel’nikov, Y.P. Smortchkova, and Y.P. Yakovlev, “Low-noise GaInAsSb/GaAlAsSb SAM avalanche photodiode in the 1.6 – 2.5 micron spectral range”, Fiber Optic Components and Reliability, SPIE Vol. 1580, pp. 308-314 (1991).
18. I. A. Andreev, M. P. Mikhailava, S. V. Mel’nikov, Yu. P Smorchkova and Yu. P. Yakovlev, “Avalanche multiplication and ionization coefficients of GaInAsSb”, Soviet Physics-Semiconductor, 25(8), 861-865, 1991.
19. T. Voronina, B. Dzhurtanov, T. Lagunova and Y. Yakovlev, “Behavior of impurities of p-type GaInSbAs solid solutions”, Soviet Physics-Semiconductor, 25(2), 171-173, 1991.
20. A. Y. Polyakov, A. G. Milnes, A. V. Govorkov, L. V. Druzhinina, I. V. Tunitskaya, and N. B. Smirnov, “Band offsets in hetrojunctions of InGaAsSb/AlGaAsSb”, Solid-State Electron, **38**(10), 525-529, 1994.
21. T. Yuan, Z. Baolin, J. Yixin, Z. Tianming, L. Shuwe, N. Yongqiang, Y. Jinshan, J. Hong and Y. Guang, “Calculation on relation of energy bandgap to composition and temperature for $Ga_xIn_{1-x}As_{1-y}Sb_y$”, *Rare Metals*, 15(3), 172-178, 1996.
22. Z. A. Shellenbarger, M. G. Mauk, M. I. Gottfried, J. D. Lesko and L. C. DiNetta, “GaInAsSb and InAsSbP photodetectors for mid-infrared wavelengths”, Proceeding of SPIE, 2999, 25-33, 1997.
23. Z. A. Shellenbarger, M. G. Mauk, J. Cox, J. South, J. Lesko, P. Sims, M. Jhabvala and M. Fortin, “Recent progress in GaInAsSb and InAsSbP photodetectors for mid-infrared wavelengths”, *Proceeding of SPIE*, **3287**, 138-145, 1998.
24. Z. A. Shellenbarger, M. G. Mauk, J. Cox, J. South, J. Lesko, P. Sims, L. DiNetta, “GaInAsSb and InAsSbP photodetectors for mid-infrared wavelengths”, Proceeding of SPIE, **3379**, 354-360, 1998.
25. T. Refaat, N. Abedin, G. Koch and U. Singh, “InGaAsSb detectors’ characterization for 2-µm CO_2 lidar/DIAL applications”, NASA Technical Publication, NASA/TP-2003-212140, 1-27, 2003.
26. O.V. Sulima, M.G. Mauk, Z.A. Shellenbarger, J.A. Cox, J.V. Li, P.E. Sims, S. Datta, and S.B. Rafol, “Uncooled low-voltage AlGaAsSb/InGaAsSb/GaSb avalanche photodetectors”, IEE Proc.-Optoelectron, Vol. 151 (1), pp. 1-5 (2004).
27. J.D. Beck, C. Wan, M.A. Kinch, J.E. Robinson, P. Mitra, F. Ma, and J.C. Campbell, “The HgCdTe electron avalanche photodiode”, presented at SPIE 49th Annual Meeting, Denver, Colorado, 2-6 August 2004 (Invited Paper).
28. O.V. Sulima, T.F. Refaat, M.G. Mauk, J.A. Cox, J. Li, S.K. Lohokare, M.N. Abedin, U.N. Singh, and J.A. Rand, “AlGaAsSb/InGaAsSb phototransistors for spectral range around 2-µm”, Electronics Letters, Vol. 40, 766-767, 2004.
29. O.V. Sulima, T.F. Refaat, M.G. Mauk, J.A. Cox, J. Li, S.K. Lohokare, M.N. Abedin, U.N. Singh, and J.A. Rand, “Novel AlGaAsSb/InGaAsSb phototransistors for spectral range 2.0 - 2.1 µm”, presented at 6th Middle-Infrared Optoelectronics Materials and Devices (MIOMD) Conference, in St. Petersburg, Russia, June 28 – July 1, 2004.
30. M.N. Abedin, T.F. Refaat, O.V. Sulima, and U.N. Singh, “AlGaAsSb/InGaAsSb heterojunction phototransistors with high optical gain and wide dynamic range”, IEEE Trans. Electron Devices, Vol. 51(12), pp 2013 - 2018 (2004).
31. M. N. Abedin, T. F. Refaat, R. P. Joshi, O. V. Sulima, M. Mauk & U. N. Singh, “Characterization and analysis of InGaAsSb detectors” Infrared Technology and Applications XXIX, Proceedings of SPIE, Vol. 5074, pp. 332-342, 2003.
32. T. Refaat, N. Abedin, G. Koch, S. Ismail, and U. Singh, “Infrared detectors characterization for CO_2 DIAL measurements”, Lidar Remote Sensing for Environmental Monitoring IV, Proceeding of SPIE, Vol. 5154, 65-73,2003.
33. M.N. Abedin, T.F. Refaat, and U.N. Singh, “Noise measurement of III-V compound detectors for 2 µm lidar/dial remote sensing applications”, Int. Journal of High Speed Electronics and Systems, Vol. **12** (2), pp. 531-540, 2002.
34. T.F. Refaat, M.N. Abedin, and U.N. Singh, “Spectral response measurements of short wave infrared detectors (SWIR)”, Int. Journal of High Speed Electronics and Systems, Vol. **12** (2), pp. 541-550, 2002.